Micropumping of liquid by directional growth and selective venting of gas bubbles†

Dennis Desheng Meng*‡ and Chang-Jin "CJ" Kim

Received 4th January 2008, Accepted 26th March 2008
First published as an Advance Article on the web 24th April 2008
DOI: 10.1039/b719918j

We introduce a new mechanism to pump liquid in microchannels based on the directional growth and displacement of gas bubbles in conjunction with the non-directional and selective removal of the bubbles. A majority of the existing bubble-driven micropumps employs boiling despite the unfavorable scaling of energy consumption for miniaturization because the vapor bubbles can be easily removed by condensation. Other gas generation methods are rarely suitable for micropumping applications because it is difficult to remove the gas bubbles promptly from a pump loop. In order to eradicate this limitation, the rapid removal of insoluble gas bubbles without liquid leakage is achieved with hydrophobic nanopores, allowing the use of virtually any kind of bubbles. In this paper, electrolysis and gas injection are demonstrated as two distinctively different gas sources. The proposed mechanism is first proved by circulating water in a looped microchannel. Using H_2 and O_2 gas bubbles continuously generated by electrolysis, a prototype device with a looped channel shows a volumetric flow rate of 4.5–13.5 nL s^{-1} with a direct current (DC) power input of 2–85 mW. A similar device with an open-ended microchannel gives a maximum flow rate of ~65 nL s^{-1} and a maximum pressure head of ~195 Pa with 14 mW input. The electrolytic-bubble-driven micropump operates with a 10–100 times higher power efficiency than its thermal-bubble-driven counterparts and exhibits better controllability. The pumping mechanism is then implemented by injecting nitrogen gas bubbles to demonstrate the flexibility of bubble sources, which would allow one to choose them for specific needs (*e.g.*, energy efficiency, thermal sensitivity, biocompatibility, and adjustable flow rate), making the proposed mechanism attractive for many applications including micro total analysis systems (μTAS) and micro fuel cells.

Introduction

Microfluidic technologies have introduced numerous exciting tools for biomedical research and practices,[1,2] such as genomics, proteomics, clinical diagnostics, pharmaceutics and drug delivery. More recently, micro power generators[3,4] have joined this family, riding on a similar technical platform. In most of those microfluidic devices, micropumps[5,6] are key components to mobilize the liquid for many microfluidic functions, including delivery, mixing, and separation of samples, reagents, or fuels. External pressure sources, whether they are bulky centrifugal pumps or smaller syringe pumps, not only served well on the early stage of microfluidic research and development but also are acceptable for many applications down to tabletop systems. However, for a small standalone (*e.g.*, handheld) *system*, it is most desirable if the pumping function is integrated in the microfluidic device to reduce space, weight and energy consumption. Only then the advantages of miniaturization can be fully exercised, opening the door for such sought-after notions as individual point-of-care systems. A true lab-on-a-chip should include all the essential capabilities including pumps in the *lab* and operate as far as energy (*e.g.*, electricity) and instructions (*e.g.*, electric signals) are provided from the outside.

Micropumps can be classified into two categories, depending on whether they have solid mechanical moving parts or not. Micropumps with moving parts[7,8] are usually straightforward in concept because of the clear analogues in the macroscopic world but tend to suffer from the exceedingly complex fabrication and difficulty in large-scale integration. Long-term reliability is also a concern due to the higher wear and tear compared with their macro-counterparts. Due to the above difficulties, micropumps free of solid mechanical moving parts have been very attractive. Most electrokinetic (*e.g.*, dielectrophoretic or electroosmotic) micropumps belong to this category. However, they are usually sensitive to the liquid medium and apt to require high voltage (usually higher than 100 V), which makes the on-chip integration difficult.

In the mean time, bubble-driven micropumps[9–11] provide a very promising solution to avoid or reduce mechanical moving parts in microfluidic systems. They typically operate at lower voltages than electrokinetic micropumps. The actuation pressure

Mechanical and Aerospace Engineering Department, University of California, Los Angeles (UCLA), 420 Westwood Plaza, Los Angeles, CA, 90095-1597, USA

† The HTML version of this article has been enhanced with colour images.

‡ Current address: Mechanical Engineering—Engineering Mechanics Department, Michigan Technological University, 815 R. L. Smith Building, 1400 Townsend Drive, Houghton, MI 49931, USA. Tel: +1 906-4873551; E-mail: dmeng@mtu.edu

is fairly high because the surface tension scales strongly in microscale.[12] Despite the advantages, thermal generation of gas bubbles by boiling, the most common approach for bubble-actuation, faces important drawbacks. Firstly, the required heat flux of boiling increases with a shrinking heater,[13] rendering the thermal bubble generation in microscale an "energy hungry" process.[14] Secondly, overheating denatures most biological large molecules (*e.g.*, DNA and protein) and may affect biomedical samples irreversibly. Thirdly, boiling is a complex thermophysical phenomenon, significantly affected by surface properties and surrounding conditions. Therefore, it is difficult to precisely predict or control the bubble growth (*i.e.*, actuation speed), resulting in considerable discrepancies caused by the fabrication process and environmental changes. Fourthly, there is a tradeoff between the generation (boiling) and collapse (condensation) of thermal bubbles. While slow heat dissipation is preferred for localized heating and efficient vapor bubbles generation, fast heat dissipation is preferred to quench the bubbles rapidly in the same device. Since natural condensation is usually far slower than active boiling, bubble collapse becomes the most time-consuming step, which leads to a low operational frequency and a slow average pumping rate. The only means to speed up is to accelerate heat dissipation, which inevitably compromises power efficiency.

Various other bubble generation approaches, such as electrolysis,[15] injection,[16] and chemical reaction,[17] have also been reported. However, removal of insoluble gas bubbles from a sealed device is much harder and slower than condensation, if possible at all.[18,19] As a result, the successful bubble-driven micropumps that do not use boiling are typically made open so that the bubbles leave the fluidic system along with the liquid being dispensed.[15–17] Even condensation itself cannot completely remove the entire vapor bubble residue within a practical time scale, and a downstream opening is usually necessary to avoid bubble clogging of the fluid loop.[20] There is no bubble-driven micropump suitable for a closed fluidic network in a miniaturized system like a micro direct methanol fuel cell (μDMFC)[21] or circular chromatography.[22] A breakthrough for the universal and prompt gas removal is highly desired to utilize bubble sources other than boiling, such as electrolysis, injection, chemical reaction, and ultrasonic cavitation. With the freedom to use any bubble generation method when designing a bubble-based micropump, one would be able to address the specific concerns of individual applications (*e.g.* energy efficiency, thermal sensitivity, biocompatibility, and adjustable flow rate).

The pumping mechanism reported in this paper employs hydrophobic nanoporous venting, a universal gas removal mechanism much faster than the existing approaches, accommodating nearly all the existing bubble generation methods for micropumping. Combined with a virtual check valve where the bubbles expand directionally, the universal venting mechanism plays a key role in the design of the proposed pumping mechanism. As the main interest of this paper, pumping is demonstrated in a closed microfluidic system, *i.e.*, a looped microchannel, by generating gas bubbles continuously without regulation. An open-ended microchannel is also tested to characterize the pumping for the static pressure head. While micropumping by electrolytic bubbles are the main interest of this paper, we also report the use of nitrogen bubbles injected from outside to demonstrate the versatility of the reported pumping mechanism. This pumping mechanism has recently been employed to design a micro direct methanol fuel cell (μDMFC) that delivers liquid fuel without an external pump,[23] using electrochemically-generated CO_2 bubbles inherent in the fuel cell.

Working principle

The working principle of this new pumping mechanism is based on two essential components: a virtual check valve for asymmetric (*i.e.*, directional) bubble growth and the hydrophobic nanoporous venting for rapid bubble removal. Furthermore, the hydrophobic surface attracts the bubbles at the hydrophilic–hydrophobic junction (*i.e.*, hydrophobic bubble capture[35]), assisting the directional displacement of the bubbles in the system. The venting site is the only hydrophobic surface in the entire microchannel system which is otherwise hydrophilic.

Virtual check valve

It is well known that a small gas bubble in a liquid-filled microchannel can effectively impede the liquid flow. Directional flow can be regulated by creating and eliminating the bubble in coordination with the desired flow directions,[9,24,25] or by placing the bubble at a channel neck where the cross-sectional area changes abruptly.[11,16,26] Because the bubble functions as if a mechanical check valve were placed in microchannel, such a functional bubble may be considered a "virtual check valve".[24,25] A simple structure of the channel neck is illustrated in Fig. 1a. When a bubble is generated adjacent to this channel neck, the meniscus on each side of the bubble can withstand a certain pressure. Considering a rectangular microchannel cross-section, the maximum pressure difference that a meniscus can withstand during the bubble growth is:

$$\Delta P_i^{\max} = 2\sigma\left(\frac{1}{h_i}+\frac{1}{w_i}\right)\cos\theta_{\text{rec}} \quad (1)$$

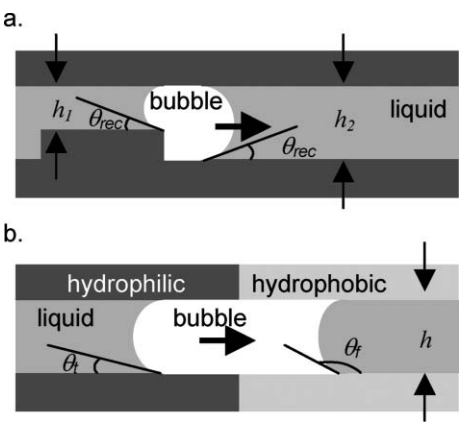

Fig. 1 Asymmetric microchannel structures for directional growth and displacement of gas bubbles in liquid. (a) A channel neck blocks a gas bubble from moving to the left and dictates it to grow only to the right, serving effectively as a virtual check valve. (b) A hydrophilic–hydrophobic junction attracts the bubble to the right, because the hydrophobic surface is energetically more favorable for the gas than the liquid.

where σ is the surface tension of liquid–gas interface, θ_{rec} is the receding contact angle of the liquid on the inner surface of the channel, h_i stands for the channel height, w_i stands for the channel width, and $i = 1,2$ represents the two sections of the microchannel. If h_1 and w_1 are smaller than h_2 and w_2 respectively, ΔP_1^{max} is larger than ΔP_2^{max}. If the pressure inside the growing gas bubble falls between these two values ($\Delta P_1^{max} > P_{bubble} > \Delta P_2^{max}$), the left meniscus remains at the channel neck, while the right meniscus slides to the right. The liquid in the larger channel is thus pushed by the expanding bubble and flows to the right. Overall, this channel neck structure effectively uses the left menisci of the bubble, providing a virtual check valve to block the leftward flows and allow rightward flows without any mechanical moving parts.

Hydrophilic–hydrophobic junction in microchannel

Virtual check valve employs asymmetric geometry to rectify the bubble growth and displace the bubbles to one direction. A similar effect of directional bubble displacement can also be induced by a change of surface energy rather than geometry. An example is the hydrophilic–hydrophobic microchannel junction shown in Fig. 1b. In this case, the angle between the front meniscus and the hydrophobic channel wall (θ_f) is larger than 90°, which exert a capillary pressure to pull the bubble rightwards. At the same time, the angle between the tail meniscus and the hydrophilic channel wall (θ_t) is smaller than 90°, which exert a capillary pressure to push the bubble rightwards. Therefore, the bubble would move rightward and pump the liquid together with it. The total rightward capillary pressure applied upon the gas bubble is:

$$\Delta P_j = -2\sigma\left(\frac{1}{h}+\frac{1}{w}\right)(\cos\theta_f - \cos\theta_t) \quad (2)$$

where σ is the surface tension of liquid–gas interface, h represents the channel height, and w represents the channel width. Along with the virtual channel neck, this hydrophilic–hydrophobic junction induces the directional displacement of the bubbles in the system.

Hydrophobic nanoporous venting (HNV)

The principle of hydrophobic venting is shown in Fig. 2. When a microchannel is covered by hydrophobic porous membrane and filled with liquid, a small meniscus will be formed at the entrance corner of a hydrophobic venting hole located on the inner surface of the microchannel. This meniscus can change its shape corresponding to the pressure difference that it withstands. The varying pressure can therefore be balanced according to Laplace–Young equation:

$$P_1 - P_0 = \frac{2\sigma}{r}\cos(180° - \alpha) \quad (3)$$

where P_1 is the pressure inside the liquid, P_0 is the ambient pressure, r is the inner diameter of the capillary, and α is the angle between the meniscus and the inner wall at the entrance into the hydrophobic capillary. Note that the definition of α is different from that of the contact angle. When P_1 increases, α increases to accommodate the pressure change. However, when α exceeds the maximum value possible for the capillary–air–liquid interface, the meniscus can no longer hold the liquid, and the liquid leaks. Therefore, the maximum pressure difference that the hydrophobic capillary can withstand (leakage onset pressure) is:

$$P_{leak} = (\Delta P)_{max} = \frac{2\sigma}{r}\cos(180° - \alpha_{max}) \quad (4)$$

The maximum value of α is determined by the advancing contact angle: $\alpha_{max} = \theta_{adv}$. If $(P_1 - P_0)$ is kept lower than this leakage onset pressure P_{leak}, the gas can be released without loss of liquid except a trivial amount of evaporation from the tiny liquid/air interface through the long and narrow pores. It is obvious that smaller r or larger θ_{adv} leads to higher leakage onset pressure, favoring hydrophobic nanopores for the purpose.

Hydrophobic venting technology was first implemented by employing lithographically microfabricated venting holes, so as to handle microfluidic samples[27] and degas for micro-dialysis devices[28] or μDMFCs.[29,30] However, the achievable leakage onset pressure of lithographically microfabricated venting holes are seriously restricted. Firstly, it is difficult to fabricate venting holes smaller than a few micrometers by standard photolithography. Secondly, the hydrophobicity of available substrate materials is usually low. Hydrophobic coating such as Teflon® [31] is usually necessary to increase the contact angle. However, coating inside these small holes tends to block them, which gets even worse for smaller holes. The uniformity of the hydrophobic coating cannot be guaranteed by simple spin-coating or dip-coating either. Moreover, if the microfabricated venting holes are arranged along the sides of the microchannel as usual,[28] the number of the venting holes is limited, and so is the venting rate. The limitation is more problematic if the size of the venting holes is further reduced, for example, to hundreds of nanometer or smaller, due to the dramatically increased gas flow resistance, which is in inverse proportion to r^4, according to the Hagen–Poiseuille equation.[32] In order to confront these challenges, we have developed hydrophobic nanoporous venting (HNV) technology[33,34] by employing commercially available hydrophobic nanoporous membranes and accordingly improving both the leakage prevention and venting rate. The pores size of this category of membranes can be as small as 100 nm in diameter, forbiddingly difficult if photolithographic microfabrication had to be used. Furthermore, no additional coating is necessary because the materials are intrinsically hydrophobic. We have reported a sandwiched membrane breather[33,34] to remove CO_2 gas bubbles generated in μDMFC. By using porous polypropylene membrane, the leakage onset pressure has been improved greatly. Successful gas removal has been achieved for both deionized

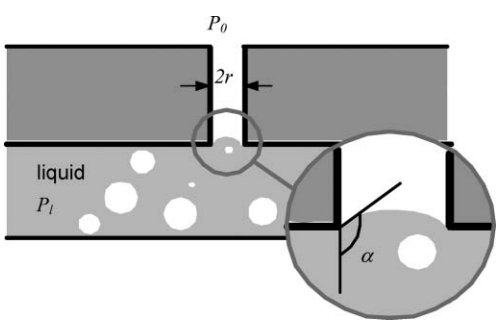

Fig. 2 A hydrophobic venting hole passes gas while blocking liquid.

(DI) water and 10 M methanol (the high-concentration fuel of μDMFC) with pressure tolerance as high as 200 kPa. Venting could be implemented in any orientation, free of gravitational effect. The HNV technology actually works for both soluble and insoluble gases, which makes it a universal gas removal approach. In comparison with the lateral configuration,[28] the membrane surface of HNV covers an entire wall of the microchannel, hosting many more venting holes and thus allowing a fast venting despite the small hole size. It should be noted that small breathing holes allow higher pressure without leakage. In all of our micropumping tests, the venting was always fast to remove all the gas bubbles generated in the device, and no gas accumulation has been observed during the uninterrupted water electrolysis. Bubble removal is hence no longer the bottleneck for pumping rate (frequency) if this venting mechanism is used. A theoretical model to determine the venting rate[30] has been developed and verified to provide a guideline for the design and optimization of breathers, as well as for the micropumps based on HNV.[41]

Pumping mechanism

The general pumping concept is schematically described in Fig. 3. To simplify the analysis, a pumping cycle is explained in three steps with a single bubble.

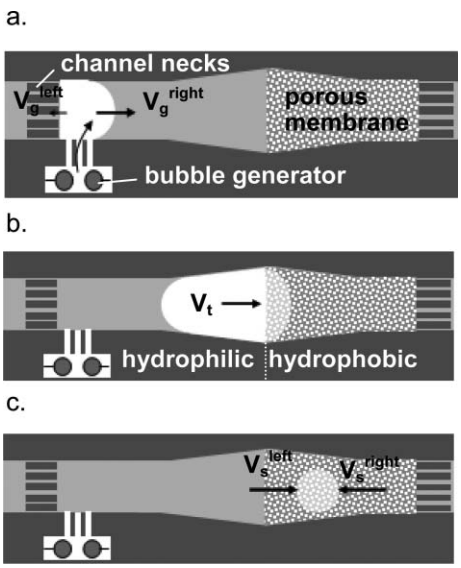

Fig. 3 The three-step concept to pump liquid by directional growth, hydrophobic capture and selective venting of gas bubble. (a) Step 1: directional bubble growth. (b) Step 2: built-in bubble displacement. (c) Step 3: symmetric bubble collapse.

Step 1. When a bubble grows near the channel necks at the entrance of a microchannel, expansion of the left meniscus is hindered by the valving effect as discussed previously. Consequently, the bubble only grows to the right and pushes the liquid rightward.

Step 2. Once the front meniscus of the bubble reaches the hydrophilic–hydrophobic junction, the surface energy difference induces a rightward displacement of the bubble as described in Fig. 1b. This energy gradient makes the hydrophobic membrane a *bubble trap*,[35] which attracts the gas bubble in much the same way as a hydrophilic patch on a hydrophobic surface traps a liquid droplet. The shape of the hydrophilic microchannel can also be designed to promote rightward bubble displacement. A diverging shape microchannel[36,37] is specified here to do so. However, since pumping is observed in a simple straight channel as well with no observable difference, we report that the diverging channel design may help but is not required to complete the pumping. The channel shape may be further optimized to improve the pumping performance, but it is beyond the current interest.

Step 3. Through the numerous tiny venting holes in the nanoporous membrane, the gas is removed selectively while the liquid is blocked, as far as the pressure difference ($P_1 - P_0$) is less than P_{leak}, the leakage onset pressure. It has been determined that P_{leak} is higher than 200 kPa for the specific nanoporous polypropylene membrane reported in this paper,[34] posing practically no danger of liquid loss with a sufficient safety margin in most applications. The liquid then flows into the membrane section of the microchannel symmetrically to fill in the space previously occupied by the gas bubble. One pumping cycle is thus completed, and a net pumping of the liquid to the right is achieved.

Although this concept is illustrated with a single bubble, the coexistence of randomly distributed multiple bubbles is acceptable for pumping as long as the venting rate of the membrane is sufficient to remove all of the bubbles promptly. Therefore, the bubble-driven pumping mechanism reported here can be generalized for continuous bubble generation. This flexibility differs from traditional thermal-bubble-driven micropumps that use pulsed power inputs to generate a vapor bubble and then turn off the heater to wait for the bubble to collapse by condensation. Continuous bubble generation without a precise modulation can significantly simplify the driving circuit, reducing both the system complexity and the power consumption. Tolerance of a bubble generation pattern also enables those challenging applications where precise regulation of a bubble generation rate is difficult (*e.g.*, chemically generated CO_2 bubbles in micro fuel cells).

Implementation: Device design and fabrication

Electrolytic-bubble-driven micropump

Electrolysis of water is chosen as the first bubble generation approach to implement the proposed bubble-driven micropumping mechanism. Electrolysis can be simply achieved by two electrodes in most aqueous solutions. Compared with boiling, electrolysis possesses several apparent advantages especially in microscale. An electrolytic-bubble-actuated microvalve has been reported to consume power of four orders of magnitude less than a similar thermal-bubble actuated microvalve.[18,38] Electrolytic bubble actuation was also reported recently to manipulate living cells,[39] a difficult feat for thermal bubble actuations. A systematic comparative study on boiling and electrolysis bubble actuation[40] also showed much lower power consumption and better controllability of the latter. Despite these advantages over thermal approaches, removal of the electrolytic bubbles has been too slow to be feasible in closed systems even with help

of catalyst. With the recently developed HNV[30] technology, we believe that the time is ripe for an electrolytic bubble pump.[41]

Pump loop configuration and fabrication

The proposed pumping concept is first implemented in a pump loop in order to demonstrate continuous liquid circulation, as required in many standalone portable microfluidic devices such as μDMFC. In addition to portability considerations, the elimination of open ends also prevents some uncertainties about the device, such as evaporation and the pressure effect of the menisci.

The construction of the test device is described with Fig. 4. The device consists of three main plates: 1. a glass substrate to support the device and allow observation of the whole pump loop from below, 2. a pump chip micromachined to form the looped microchannels, and 3. a membrane holder to keep hydrophobic nanoporous membranes on the pump chip. The pump chip and membrane holders were all fabricated from the same 400 μm-thick (100) silicon wafer by deep reactive ionic etching (DRIE). On the pump chip, the microchannel loop was lithographically defined by DRIE. Once the etching reached the desired depth, most part of the microchannel was protected with polyimide tape, while the portions for the breather, the reservoir and the connection ports were allowed to etch through. After DRIE and subsequent piranha cleaning, the pump chip was anodically bonded to a piece of Pyrex® glass. Then the hydrophobic nanoporous membranes were sandwiched between the pump chip and membrane holders. The holders were bonded on the pump chip by epoxy adhesive to form a breather and a gas-permeable reservoir so as to avoid the introduction of gas bubbles during priming or operation. During the bonding, the holder chip and the pump chip were aligned using the through-holes made on them, assisted by strong illumination from below. Details of this alignment and bonding technique were described previously.[34,42] Two platinum wires were inserted into the "bubble source" position as the electrodes for electrolysis. The finished pump loop is subsequently connected to a syringe *via* an apparatus consisting of tubes, fittings, and adapters.

Experimental results

Verification of liquid circulation in pump loop

The working fluid, Na_2SO_4 aqueous solution (~0.2 M), was filled into the completed device by a syringe. The presence of ions in the solution can lower the voltage drop between the anode and cathode and therefore ease the electrochemical reaction. During the priming process, it was common for gas bubbles to be introduced into the loop accidentally.[43] The reservoir was therefore covered with a venting membrane so that these bubbles can be removed automatically, allowing the pump loop free of bubbles and avoiding bubble-clogging problems.[44,45] Therefore, the device reported herein does not require degassing of the liquid[46] or vacuum priming.[47] After the pump loop was filled with working fluid, a mechanical valve between the device and the syringe was closed to isolate them from each other. A DC voltage was then applied between the two platinum electrodes. Substantial electrolysis was observed when the voltage was increased to 10 V or above. For thermal-bubble-driven micropumps,[10,11] certain patterns of pulsed power input is typically necessary because the boiling needs to be halted to allow the condensation of vapor bubbles. The regulation of voltage/power input requires a driving circuit, introducing a complexity to the system. Since the continuous bubble removal is much faster than the bubble generation in our device, the power input does not need to be pulsed or regulated. Accordingly, DC voltage was used to generate gas bubbles continuously. In this way, pumping efficiency can be improved and the driving circuit simplified, providing considerable benefits for the portable microfluidic devices.

Under an operation voltage of 20 V_{dc}, three areas in the pump loop (A, B and C in Fig. 4) were observed to verify the circulation of liquid. Bubble growth, displacement, and removal in the pumping section (area A in Fig. 4) are demonstrated in Fig. 5. Fine bubbles generated on the electrodes merged into larger bubbles first (Fig. 5a). Since the leftmost bubble was blocked by the channel neck to form a virtual check valve, all the bubbles only grew rightward (Fig. 5b). Both the surface energy difference and the shape of the microchannel facilitated

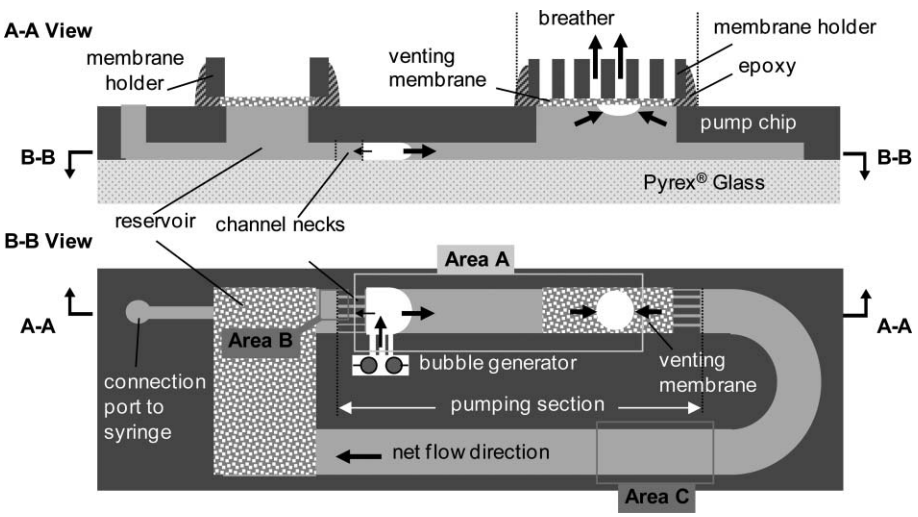

Fig. 4 Configuration of the main device with a looped microchannel, illustrating main components and areas for observation.

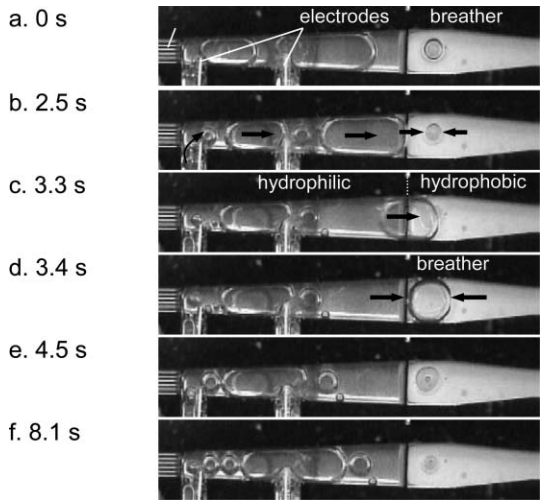

Fig. 5 Sequential pictures of bubble growth, displacement, and collapse in pumping section (corresponding to Area A in Fig. 4).

the rightward bubble displacement (Fig. 5c) and delivered the leading bubble to the venting membrane (Fig. 5d). After the leading bubble reached the venting membrane (noted "breather" in the figure), it started to be removed and collapsed rapidly (Fig. 5c–e). Meanwhile, bubbles were continuously generated by the electrodes to start the subsequent pumping cycles. The liquid was pushed rightward along with the bubbles during the bubble growth and displacement phases, rendering a net rightward flow.

In order to verify the liquid circulation more concretely, the fluid uptake from the reservoir was observed in Area B of Fig. 4. Fluorescent particles (4 μm in diameter) were mixed into the working fluid to visualize the flow. Fig. 6 shows the video sequence of fluid uptake captured by a fluorescent microscope. The flow close to the inlet of the channel neck was found to be essentially unidirectional with occasional momentary stops. The unidirectional fluid uptake proved that the fresh liquid reactant from the reservoir can be supplied to the microreactor by using

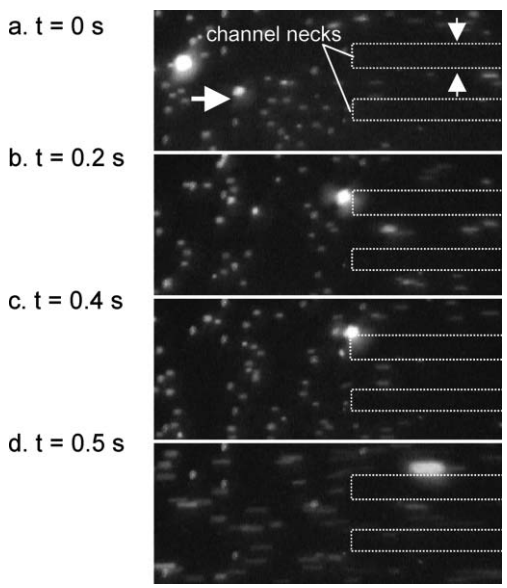

Fig. 6 Fluid uptake from reservoir (corresponding to Area B in Fig. 4).

this pumping approach. For example, in μDMFC, this means a constant supply of fresh methanol. The liquid circulation of the whole pump loop is thus confirmed by the manifestation of bubble growth, displacement, and removal in the active pumping section as well as the fluid uptake from the reservoir into the pumping section.

Characterization of pump loop

The microscopic particles in the fluid was also employed to quantitatively characterize the flow in the pump loop by a simplified micro particle image velocimetry (μ-PIV).[48] Area C in Fig. 4 has been chosen to perform velocimetry. The volumetric flow rate can be calculated by multiplying the flow velocity with cross-sectional area (600 μm × 300 μm). Fig. 7 demonstrates the particle displacement under 20 V_{dc} input voltage. Particle clusters were used to measure the flow velocity because they can be distinguished easily. As expected, the flow was measured pulsatile in nature, and a brief backflow was observed in each pumping cycle (Fig. 7c–e). Nevertheless, a definite net flow to the designed direction was verified yet again. It was noticed that the brief backflow observed in Area C was not observed in Area B. However, this difference in the flow pattern within the same fluidic loop can be explained. Again, we assume only one bubble in the whole pump loop to simplify the explanation. The practical system with multiple bubbles will exhibit accumulative effect of the single bubble argument to follow.

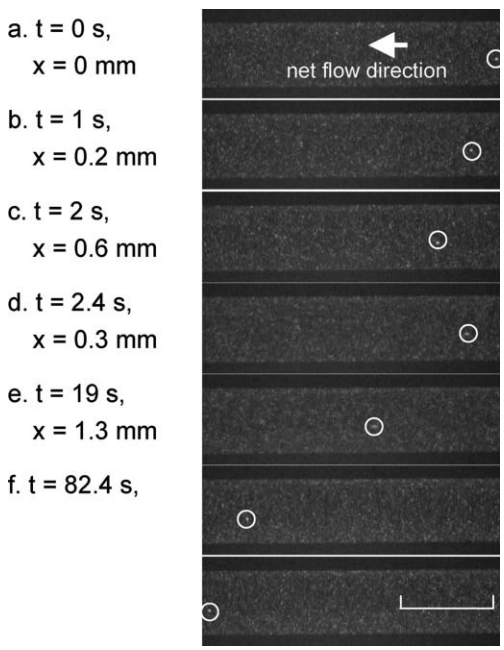

Fig. 7 Micro-PIV to determine the flow rate (corresponding to Area C in Fig. 2).

The flows between the reservoir and the channel necks (Fig. 6, or Area B in Fig. 4) were expected to be directional, because the virtual check valve blocks the leftward bubble growth effectively. When the bubble is in either the *displacement* or the *removal* phase, the induced flow was forward (*i.e.*, rightward). During the *bubble growth* phase, on the other hand, the flow would only

stop but not reverse to the left. The overall flows in Area A were not uniform but unidirectional as confirmed by the experiments.

In contrast, the flows downstream of the venting section (Fig. 7, or Area C in Fig. 4) were expected to include momentary reversals, because there was no valving mechanism to control the displacement of the forward (right) meniscus of the bubble in Area A. During the *growth* and *transportation* phases, the induced flow in Area C was forward (*i.e.*, leftward). When the leading bubble was in the *removal* phase, on the other hand, the flow might reverse (*i.e.*, rightward), inducing a minor and momentary backflow. The overall flows in Area C were therefore pulsatile with brief reversals as observed in the experiments.

Different operation voltages were used to characterize the performance of the reported pumping mechanism by determining the relationship between driving voltage/power and volumetric flow rate in the test device. The results are summarized in Table 1. This result has indicated that the flow rate was well controlled by the power input and adjustable over a broad range. The reason for this feature is that the electrolytic bubble generation rate is reliably proportional to the input current. High repeatability of this correlation has indeed been observed during the experiments, suggesting that the pumping rate can be both measured from and controlled by the current. This unique feature may also be employed to stabilize the pumping rate by using feedback control. In comparison, generation of thermal bubbles (boiling) is complicated by many factors such as surface properties, heat transfer boundary conditions and transient (*i.e.*, time dependent) variables. Precise control of thermal-bubble-driven micropumps is much more difficult.

It is worth noticing that the theoretical equilibrium potential to generate hydrogen and oxygen by electrolysis is 1.23 V. The practical minimum voltage for electrolysis actuation has been reported to be around 3 V.[15,39] Our minimum operation voltage of ~10 V is substantially larger than both of them because the distance between our two electrodes (inserted Pt wires) is around 2 mm. The micromachined electrodes are expected to be much closer to each other and operate at a much lower voltage, leading to a much higher power efficiency.

Characterization of pumping in an open-end channel

Another important characteristic of a micropump is the pressure head and the corresponding flow rate that the pump can provide. Direct measurement of pressure head in the looped microchannel would require integrated pressure sensors, significantly increasing the complexity of the device. In this study, instead, the pressure head was measured with the same micropump structure built in an open-ended channel configuration, avoiding the added complexity an integrated device would have required. Fig. 8 shows the open-ended pump fabricated by the same fabrication procedure as its looped counterpart. Through-holes were etched at the two ends of this straight channel, with two glass tubes attached on by epoxy. Working fluid (water with Na_2SO_4) was introduced slowly from the top of the inlet tube by a syringe. After the meniscus of the outlet tube rose to a certain height and stabilized, DC voltage was applied to start the pumping. The displacement of the inlet/outlet menisci during the whole process was recorded by a digital video system.

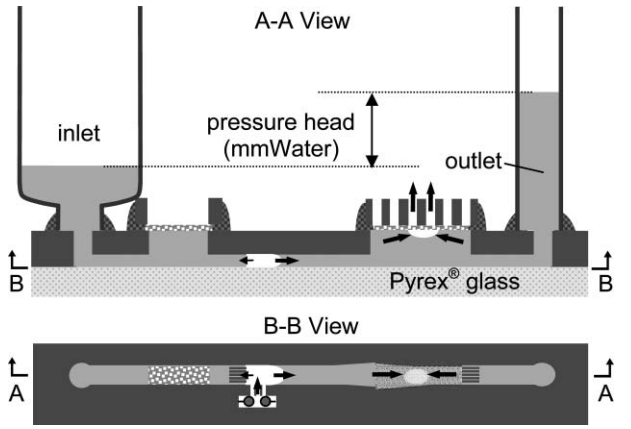

Fig. 8 Configuration of the device with an open-ended microchannel and accompanying setup for characterization.

The velocity of outlet meniscus was measured from the video clips. The volumetric pumping rate can be calculated by multiplying the meniscus velocity by the cross-sectional area of the outlet tube. Since the cross-section area of the inlet tube was much larger than the outlet tube, the inlet meniscus remained roughly same during pumping. The position of the outlet meniscus was therefore used to determine the pressure head at any given time. Under an input voltage of 20 V_{dc}, the relationship between the flow rate and the pressure head was obtained experimentally and shown in Fig. 9. When the pump was just turned on, the pressure head was close to zero, and the flow rate was the highest. However, the first two data points have been discarded because the pumping was not stabilized yet. Before the first bubble was removed, the flow rate only reflected the bubble growth rate. The practical maximum pumping rate of ~65 nL s^{-1} was obtained against a back pressure of ~50 Pa. One data point was recorded whenever the height of the outlet water column increased 1 mm (equivalent to 11.8 Pa).

Table 1 Control of the volumetric flow rate in pump loop

Voltage/V	10	20	30	40
Average current/mA	0.20	0.69	1.32	2.13
Average power/mW	2.0	13.8	39.6	85.2
Particle velocity/μm s^{-1}	25	33	50	75
Volumetric flow rate/nL	4.5	5.9	9.0	13.5

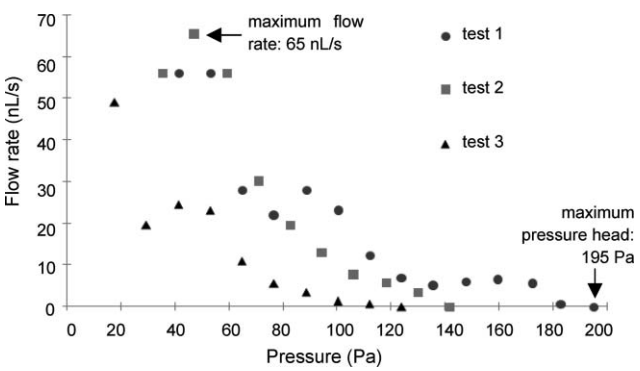

Fig. 9 Flow rate *vs.* pressure head measured with open-end channel devices.

After the outlet meniscus stayed at the same level for more than 5 min, the flow rate was considered to be zero. The test was repeated several times, with three representative data sets shown in Fig. 9. The maximum pressure head of ~195 Pa was obtained at this point. Three situations or their combinations would lead to the maximum pressure head. Firstly, the size of the channel necks (50 μm) for virtual check valve might not be small enough to block the leftmost bubble. Secondly, the bubble capturing and displacement mechanism may fail due to the limited capillary pressure difference across the hydrophilic–hydrophobic microchannel junction. Thirdly, the square cross-section of the hydrophilic microchannel allows the liquid to fill the corners.[49] The liquid can therefore leak through the corners due to the back pressure (pressure head). The overall flow rate would therefore reach zero when the pumped flow is negated by the leakage flow through the corners. In our experiments, we observed that the pumping section (Area A of Fig. 4) still worked properly without any bubble escaping to Area B or stopping at the hydrophobic-hydrophilic microchannel junction when the pumping rate dropped to zero. In other words, the pumping ceased before the *virtual check valve* or the *bubble trap* failed. Therefore, we conjecture that it was the third situation that determined the maximum pressure head in our case. The use of round microchannels would alleviate the backward leakage flow. At the same time, reducing the size of the microchannel and the channel necks would further increase the maximum pressure of the pump if the backward leakage flow can be effectively prevented. However, smaller microchannel means significantly increased flow resistance, and round shape microchannel is challenging for microfabrication. Therefore, optimum size and shape of the micropump components should be determined for specific applications, which is beyond the scope of this paper.

Under 20 V_{dc} input voltage, the average current during pumping was measured as 0.7 mA. Therefore, the power consumption of the pump in this test was 14 mW. In order to achieve the similar maximum flow rate in thermal-bubble-driven micropumps, power consumption above several hundred mW was usually required.[8,10,11,14] Therefore, the efficiency of this electrolytic-bubble-driven miropump was found to be approximately 10–100 times better than those of thermal-bubble-driven micropumps.

Exploration of more bubble sources

The electrolytic-bubble-driven pump shows several significant improvements over traditional thermal-bubble-driven pumps. However, there are still many bubble generation approaches other than the above two. Although the basic pumping mechanism enabled by HNV technology is expected to work with any type of bubbles, one should test the validity and assess the characteristics, such as device fabrication, energy efficiency, thermal sensitivity, biocompatibility and flow rate adjustability, through further studies for each type.

One example of the potentially important bubble generation approaches is "gas injection", which is more generic than boiling or electrolysis because it imposes no limit on the nature or composition of liquid to be pumped. Therefore, the pumping mechanism can be expanded to liquid samples that are nonconductive or too sensitive for boiling and electrolysis (*e.g.*, explosive). This advantage of the injection micropumping approach can also benefit biomedical applications.[16] It is well-known that most proteins and DNA can be denatured at the boiling temperature of the biomedical aqueous solution. At the same time, they are usually electrically charged and therefore responsive to a strong electrical field. Therefore, both boiling and electrolysis may chemically modify biomedical molecules. In comparison, injection of an inert gas will not affect biomedical molecules chemically, electrically, or thermally, and thus holds the potential for better bio-comparability. A proof-of-concept device we fabricated is presented schematically in Fig. 10. The configuration of the pumping section was the same as that of the looped electrolytic-bubble-driven pump, with channel necks for the asymmetric bubble growth, a hydrophilic–hydrophobic microchannel junction for the directional bubble displacement, and a venting membrane to remove bubbles. The gas bubbles were injected from an external nitrogen gas tank through the gas injection channel. An external mechanical valve was used to control gas injection manually. Two large openings were etched into the pump chip at the two ends of the pump channel as inlet and outlet reservoirs. The surfaces of reservoirs were treated with hexamethyldisilazane (HMDS) (contact angle ~80°), so that the capillary effect of the reservoirs was minimized.

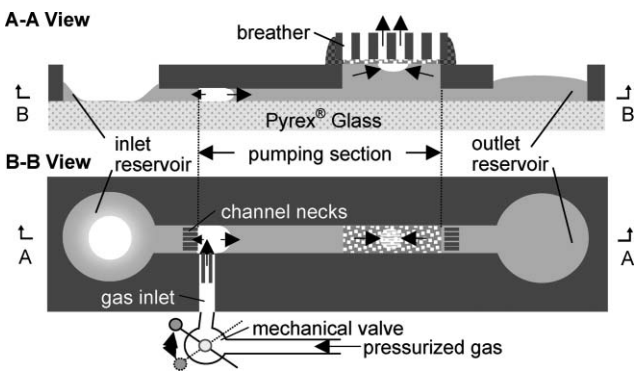

Fig. 10 Pumping by directional injection and hydrophobic venting of gas bubbles.

Before testing, DI water with black ink was deposited into the inlet reservoir by pipette. The hydrophilic microchannel in the pumping section was automatically filled with the liquid due to capillary effect. The front meniscus of liquid stopped when it contacted the hydrophobic membrane of the breather. Then the mechanical valve was opened to inject gas into the pumping section. The gas bubble expanded as Fig. 11b and c show. On the right-hand side of this gas bubble, the liquid was pushed to the outlet reservoir. Meanwhile, the left meniscus of the injected gas bubble was stopped at the channel necks between the reservoir and the pumping section, so no liquid (nor gas) was passed through the channel necks towards the left. After the front meniscus of the gas bubble reached the venting membrane of the breather, the mechanical valve was closed. The bubble started to shrink immediately because the gas was removed through the venting holes on the membrane (Fig. 11d). Since the hydrophobic membrane of the breather also works as a bubble trap, the bubble was held to the venting section (marked as "breather" in the figure) while being removed (Fig. 11e and f).

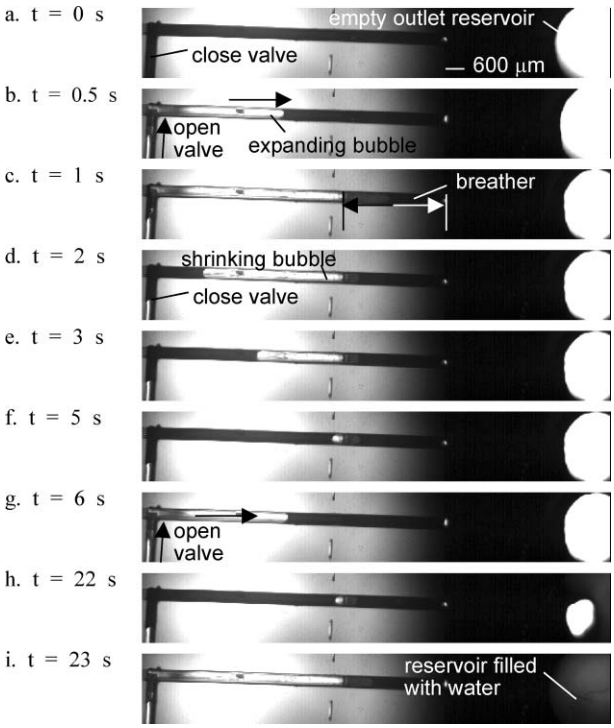

Fig. 11 Visualization of pumping effect using injected gas.

Liquid filled in spontaneously as the left meniscus of the bubble moved to the right during the venting. Once the bubble was completely removed, the mechanical valve was opened again to start the next pumping cycle (Fig. 11g). Fig. 11i shows that the outlet reservoir was completely filled with water after four pumping cycles.

Two additional observations have further confirmed that the pumping effect were induced by gas injection and venting instead of capillary or hydraulic pressure. Firstly, if the mechanical valve was closed during any time of the pumping phases, the liquid delivery to the outlet reservoir stopped accordingly. Secondly, most of the liquid in the inlet reservoir were pumped to the outlet, leaving the inlet reservoir almost completely dry, except in the corners (as illustrated in Fig. 10).

The recently developed micro gas generators[17,50] can be employed to replace the external gas tank and enable the on-chip integration. By integrating the on-chip gas injection source, a lab-on-a-chip operated by a fully biocompatible micropumping mechanism can be anticipated.

Discussion

The reported pumping mechanism appears most promising when applied to a μDMFC, where the gas bubbles are constantly generated by the electrochemical reaction inherent with the fuel cell operation. Since the bubble generation is intrinsic, it is even possible to pump liquid fuel without electrolysis, which means that the electrodes and power input are not necessary any more. Most importantly, by eliminating the need for the external pump and gas/liquid separator, configuration of the μDMFC system can be greatly simplified, a critical advantage for miniaturization. The feasibility of our micropumping mechanism for μDMFC applications has been proven by circulation of a liquid fuel by CO_2 gas bubbles from the fuel cell reaction.[23]

Hydrophobic nanoporous venting can also be employed in bubble-driven micropumps that use mechanical valves[8] to improve the performance (*e.g.* pressure head) over the valveless micropumps. The benefits of flexible bubble sources on energy efficiency, thermal sensitivity, biocompatibility, and controllability are still applicable in those cases.

Built on the micropumping concept first introduced by Meng and Kim,[41] this paper presents a full account of the technology, including theoretical/analytical ground, design details, more experimental results and characterization, and pumping demonstration with multiple bubble generation methods. In the mean time, Cheng and Liu recently reported a micropumping similar in concept: driven by a directional movement of electrolytic bubbles followed by its removal. The apparent similarity calls for further discussion for differences. They employed "periodic generation of electrolytic bubbles" using the electrodes patterned directly on chip and demonstrated operation in an open-ended microchannel.[51] The directional displacement of bubbles was induced by a roughness gradient of a hydrophobic surface, and the gas was removed through a lithographically fabricated breather placed lateral to the microchannel. In comparison, overall, our paper focuses on the verification of a liquid circulation in a looped microchannel by continuous bubble generation, with standalone lab-on-a-chip closed systems in mind, such as μDMFC and circular chromatography. The key components employed by the two approaches are also different. First, for bubble transportation, our device uses an abrupt surface energy change across the hydrophilic–hydrophobic junction in the channel (Fig. 3) (*vs.* a gradient of surface energy employed by Cheng and Liu[51]). According to eqn (3), $(\cos\theta_f - \cos\theta_t)$ would be the most important factor to determine the surface free energy difference and eventually the maximum pressure head in a microchannel of the same size and shape. The abrupt hydrophilic–hydrophobic junction is expected to generate a greater contact angle difference (*i.e.*, larger $(\cos\theta_f - \cos\theta_t)$), compared with the roughness gradient on the structured hydrophobic surface. Second, we use nanoscale pores through a hydrophobic membrane, which demonstrated a high leakage-prevention pressure of above 200 kPa for both water and 10 M methanol[34] (*vs.* the microscale structures lateral to the channel demonstrating 17.9 kPa for water[51]). Despite the small pore size, the overall venting is still fast enough to promptly and completely remove all the electrolytically-generated gas bubbles in all of our experiments, because there are numerous pores over a large membrane area. Third and perhaps most importantly, we employ a channel neck (Fig. 1) to block the backward displacement of gas bubbles. This virtual check valve assures a unidirectional bubble displacement even in the hydrophilic microchannel of our device. The channel neck with an abrupt geometry is especially important for μDMFC application, because contact angle hysteresis on hydrophobic surface increases significantly when methanol is added to water.[34] The bubble/liquid displacement solely relying on roughness gradient of hydrophobic surface is expected to face a challenge in μDMFC. Furthermore, the hydrophilic–hydrophobic junction continues to function in μDMFC because it tolerates the effect of added methanol content. The feasibility of our micropumping mechanism for μDMFC applications has

been proven by circulation of a liquid fuel by CO_2 gas bubbles from the fuel cell reaction.[23] In terms of operation, our device has been tested for a continuous electrolysis (*i.e.*, DC input) as well as for a μDMFC system with a constant CO_2 gas bubble generation without any electrical regulation such as the periodic generation of electrolytic bubbles.[51] Lastly, no "choking or sticking of bubbles"[51] was observed in our devices, most likely because the bubble displacement paths in our devices are in a hydrophilic microchannel. Bubbles in a hydrophobic microchannel filled with an aqueous liquid show a stronger tendency to block or choke the flows than in a hydrophilic microchannel. In our device, bubbles only travel in the hydrophilic channel. No bubble displacement is required within the hydrophobic microchannel, which is simply used to capture bubbles and remove them.

Conclusion

This paper has proposed, demonstrated, and characterized a bubble-driven micropumping mechanism to circulate liquid in a looped microchannel by continuously generating gas bubbles without any regulation. The micropumping mechanism features three key components: a virtual check valve to rectify the direction of the bubble growth, a hydrophilic–hydrophobic microchannel junction to induce directional bubble displacement, and a rapid removal of insoluble gas bubbles by HNV. HNV should be considered as a universal gas removal method, which allows the design of such a micropump with virtually any bubble generation approach suitable for specific applications. We have demonstrated that our micropumping mechanism can accommodate multiple gas generation methods, with water electrolysis, injection of inert gas, and chemical reaction (*e.g.*, μDMFC) as examples. Compared with the commonly used thermal-bubble-driven micropumps, the electrolytic-bubble-driven micropump introduced in this paper achieved a similar volumetric flow rate with 10–100 times higher power efficiency, which can be further improved by reducing the gap between the electrodes. Being correlated to the current, the pumping rate has been proved to be variable and directly controlled by the input current. Electrolysis is more compatible with biological solutions over boiling, making the electrolytic-bubble-pump very promising for biomedical lab-on-a-chip applications. A preliminary investigation has also proved that the proposed pumping mechanism can utilize injected gas, which has the potential to be more generic and free of any chemical, electrical, or thermal effect on biomedical liquid samples. The freedom to choose any type of bubble generation allows for the design of an optimum bubble-driven micropump for a given application.

Acknowledgements

This work was supported by the Defense Advanced Research Projects Agency (DARPA) Micro Power Generation (MPG) Program and the UCLA Faculty Research Grant. The authors wish to thank Professors C.-M. Ho, C. Y. Wang, X. Zhang, X. Zhong, T. Cubaud, T. J. Yen, Y. Lu, as well as Drs G.Q. Lu, M. Tatineni, and W. J. Shen for their discussion and help. Ms A. Lee and Mr B. Van Dyk are also appreciated for their editorial assistance.

References

1 D. R. Meldrum and M. R. Holl, *Science*, 2002, **297**, 1197–1198.
2 P.-A. Auroux, D. Iossifidis, D. R. Reyes and A. Manz, *Anal. Chem.*, 2002, **74**, 2637–2652.
3 S. M. Mitrovski and R. G. Nuzzo, *Lab Chip*, 2006, **6**, 353–361.
4 C. M. Moore, S. D. Minteer and R. S. Martin, *Lab Chip*, 2005, **5**, 218–225.
5 D. J. Laser and J. G. Santiago, *J. Micromech. Microeng.*, 2004, **14**, R35–R64.
6 N.-T. Nguyen, X. Huang and T. K. Chuan, *J. Fluids Eng.*, 2002, **124**, 384–392.
7 J. Xie, J. Shih, Q. Lin, B. Yang and Y.-C. Tai, *Lab Chip*, 2004, **4**, 495–501.
8 S. Zimmermann, J. A. Frank, D. Liepmann and A. P. Pisano, in *Proc. the 17th IEEE Int. Conf. on Micro Electro Mechanical Systems*, Maastricht, The Netherlands, 2004, pp. 462–465.
9 T. K. Jun and C.-J. Kim, *J. Appl. Phys.*, 1998, **83**, 5658–5664.
10 J.-H. Tsai and L. Lin, *J. Microelectromech. Syst.*, 2002, **11**, 665–671.
11 X. Geng, H. Yuan, H. N. Oguz and A. Prosperetti, *J. Micromech. Microeng.*, 2001, **11**, 270–276.
12 C.-J. Kim, in *Proc. Int. Semiconductor Device Research Symp.*, Charlottesville, VA, 1999, pp. 481–484.
13 M. E. Steinke and S. G. Kandlikar, *J. Heat Transfer*, 2004, **126**, 518–526.
14 L. Lin, *Microscale Thermophys. Eng.*, 1998, **2**, 71–85.
15 D. A. Ateya, A. A. Shah and S. Z. Hua, *Rev. Sci. Instrum.*, 2004, **75**, 915–920.
16 N. R. Tas, J. W. Berenschot, T. S. J. Lammerink, M. Elwenspoek and A. v. d. Berg, *Anal. Chem.*, 2001, **74**, 2224–2228.
17 Y. H. Choi, S. U. Son and S. S. Lee, *Sens. Actuators, A*, 2004, **111**, 8–13.
18 A. P. Papavasiliou, A. P. Pisano and D. Liepmann, in *Tech. Dig. the 11th Int. Conf. on Solid-State Sensors, Actuators and Microsystems*, Munich, Germany, 2001, pp. 940–943.
19 H. Suzuki and R. Yoneyama, *Sens. Actuators, B*, 2003, **96**, 38–45.
20 J.-H. Tsai and L. Lin, *Sens. Actuators, A*, 2002, **97–98**, 665–671.
21 T. J. Yen, N. Fang, X. Zhang, G. Q. Lu and C. Y. Wang, *Appl. Phys. Lett.*, 2003, **83**, 4056–4058.
22 S. Debesset, C. J. Hayden, C. Dalton, J. C. T. Eijkel and A. Manz, *Lab Chip*, 2004, **4**, 396–400.
23 D. D. Meng and C.-J. Kim, in *Proc. the 20th IEEE Int. Conf. on Micro Electro Mechanical Systems*, Kobe, Japan, 2007, pp. 85–88.
24 F.-G. Tseng, C.-J. Kim and C.-M. Ho, *J. Microelectromech. Syst.*, 2002, **11**, 427–436.
25 F.-G. Tseng, C.-J. Kim and C.-M. Ho, *J. Microelectromech. Syst.*, 2002, **11**, 437–447.
26 F. T. Brown, in *the 1993 ASME winter annual meeting (micromechanical systems 1993)*, New Orleans, LA, 1993, pp. 21–33.
27 K. Hosokawa, T. Fujii and I. Endo, *Anal. Chem.*, 1999, **71**, 4781–4785.
28 Z. Yang, S. Matsumoto and R. Maeda, *Sens. Actuators, A*, 2002, **95**, 274–280.
29 D. D. Meng, J. Kim and C.-J. Kim, in *Proc. the 16th IEEE Int. Conf. on Micro Electro Mechanical Systems*, Kyoto, Japan, 2003, pp. 534–537.
30 D. D. Meng, J. Kim and C.-J. Kim, *J. Micromech. Microeng.*, 2006, **16**, 419–424.
31 http://www.dupont.com/teflon/af/.
32 C. Schaschke, *Fluid Mechanics: Worked Example for Engineers*, Institution of Chemical Engineers (IChemE), 1998.
33 D. D. Meng, T. Cubaud, C.-M. Ho and C.-J. Kim, in *Tech. Dig. Solid State Sensor, Actuator and Microsystems Workshop*, Hilton Head Island, SC, 2004, pp. 141–144.
34 D. D. Meng, T. Cubaud, C.-M. Ho and C.-J. Kim, *J. Microelectromech. Syst.*, 2007, **16**, 1403–1410.
35 D. D. Meng and C.-J. Kim, in *Proc. 2004, ASME Int. Mechanical Engineering Congress and Exposition*, Anaheim, CA, 2004, CD: IMECE 2004-62182.
36 M. J. Jensen, G. Goranović and H. Bruus, *J. Micromech. Microeng.*, 2004, **14**, 876–883.
37 U.-C. Yi and C.-J. Kim, *Sens. Actuators, A*, 2004, **114**, 347–354.
38 A. P. Papavasiliou, D. Liepmann and A. P. Pisano, in *Proc. 1999 ASME Int. Mechanical Engineering Congress and Exposition*, Anaheim, CA, 1999, pp. 435–440.

39 C.-T. Ho, R.-Z. Lin, H.-Y. Chang and C.-H. Liu, *Lab Chip*, 2005, **5**, 1248–1258.
40 D. D. Meng, Y. Ju and C.-J. Kim, in *Tech. Dig. the 13th Int. Conf. on Solid-State Sensors, Actuators and Microsystems*, Seoul, Korea, 2005.
41 D. D. Meng and C.-J. Kim, in *Proc. the 18th IEEE Int. Conf. on Micro Electro Mechanical Systems*, Miami, FL, 2005, pp. 423–426.
42 D. D. Meng, PhD dissertation, University of California, Los Angeles (UCLA), 2005.
43 P. Gravesen, J. Branebjerg and O. S. Jensen, *J. Micromech. Microeng.*, 1993, **3**, 168–182.
44 M. J. Jensen, MSc thesis, Technical University of Denmark (DTU), 2002.
45 A. Kawahara, P. M.-Y. Chung and M. Kawaji, *Int. J. Multiphase Flow*, 2002, **28**, 1411–1435.
46 A. Olsson, P. Enoksson, G. r. Stemme and E. Stemme, *J. Micromech. Microeng.*, 1996, **6**, 87–91.
47 I. D. Johnston, M. C. Tracey, J. B. Davis and C. K. L. Tan, *Lab Chip*, 2005, **5**, 318–325.
48 M. Raffel, C. Willert and J. Kompenhans, *Particle Image Velocimetry*, Springer-Verlag, Berlin, 1998.
49 R. F. Probstein, *Hysiochemical Hydrodynamics—An Introduction*, Wiley-Interscience Publication, 1994.
50 C.-C. Hong, S. Murugesan, S. Kim, G. Beaucage, J.-W. Choi and C. H. Ahn, *Lab Chip*, 2003, **3**, 281–286.
51 C.-M. Cheng and C.-H. Liu, *J. Microelectromech. Syst.*, 2007, **16**, 1095–1105.

